Naval Research Laboratory

Washington, DC 20375-5320

NRL/MR/7634--20-10,050

Detector Selection Methodology for the Triple-Tiny Ionospheric Photometer (Tri-TIP) Instrument

Bruce A. Fritz

NRC Postdoctoral Research Associate
Washington, DC

Scott A. Budzien
Andrew W. Stephan
Kenneth F. Dymond
Charles M. Brown
Andrew C. Nicholas

Geospace Science and Technology Branch
Space Science Division

September 21, 2020

REPORT DOCUMENTATION PAGE

Form Approved OMB No. 0704-0188

1. REPORT DATE *(DD-MM-YYYY)*
21-09-2020

2. REPORT TYPE
NRL Memorandum Report

3. DATES COVERED *(From - To)*
01/01/2019 – 12/01/2019

4. TITLE AND SUBTITLE
Detector Selection Methodology for the Triple-Tiny Ionospheric Photometer (Tri-TIP) Instrument

5a. CONTRACT NUMBER

5b. GRANT NUMBER

5c. PROGRAM ELEMENT NUMBER

6. AUTHOR(S)
Bruce A. Fritz*, Scott A. Budzien, Andrew W. Stephan, Kenneth F. Dymond, Charles M. Brown, and Andrew C. Nicholas

5d. PROJECT NUMBER

5e. TASK NUMBER
62435N

5f. WORK UNIT NUMBER
1F44

7. PERFORMING ORGANIZATION NAME(S) AND ADDRESS(ES)
Naval Research Laboratory
4555 Overlook Avenue, SW
Washington, DC 20375-5320

8. PERFORMING ORGANIZATION REPORT NUMBER
NRL/MR/7634--20-10,050

9. SPONSORING / MONITORING AGENCY NAME(S) AND ADDRESS(ES)
Office of Naval Research
One Liberty Center
875 N. Randolph Street, Suite 1425
Arlington, VA 22203-1995

10. SPONSOR / MONITOR'S ACRONYM(S)
ONR

11. SPONSOR / MONITOR'S REPORT NUMBER(S)

12. DISTRIBUTION / AVAILABILITY STATEMENT
DISTRIBUTION STATEMENT A: Approved for public release; distribution is unlimited.

13. SUPPLEMENTARY NOTES
* NRC Postdoctoral Research Associate

14. ABSTRACT
The Geospace Science and Technology Branch have developed a new class of compact, high-sensitivity three-channel photometers for ionospheric remote sensing from CubeSats and other platforms. The Triple Tiny Ionospheric Photometer (Tri-TIP) improves upon the original TIP instruments by simultaneously monitoring 2 optical and 1 background noise channels through the use of a beam splitter. Additionally, Tri-TIP fits within a 1-unit (1U) CubeSat form factor. This report details the methodology for selecting suitable detectors for use within the Tri-TIP instrument.

15. SUBJECT TERMS

16. SECURITY CLASSIFICATION OF: a. REPORT	b. ABSTRACT	c. THIS PAGE	17. LIMITATION OF ABSTRACT	18. NUMBER OF PAGES	19a. NAME OF RESPONSIBLE PERSON
Unclassified Unlimited	Unclassified Unlimited	Unclassified Unlimited	Unclassified Unlimited	26	Bruce Fritz
					19b. TELEPHONE NUMBER *(include area code)* (202) 404-1102

Standard Form 298 (Rev. 8-98)
Prescribed by ANSI Std. Z39.18

UNCLASSIFIED//DISTRIBUTION A

This page intentionally left blank.

CONTENTS

FIGURES

TABLES

This page intentionally left blank.

EXECUTIVE SUMMARY

The Geospace Science and Technology Branch have developed a new class of compact, high-sensitivity three-channel photometers for ionospheric remote sensing from CubeSats and other platforms. The Triple Tiny Ionospheric Photometer (Tri-TIP) improves upon the original TIP instruments by simultaneously monitoring two optical and one background noise channels through the use of a beam splitter. Additionally, Tri-TIP fits within a 1-unit (1U) CubeSat form factor. This report details the methodology for selecting suitable detectors for use within the Tri-TIP instrument.

Laboratory tests were conducted at the U.S. Naval Research Laboratory (NRL) to characterize the performance of commercial Hamamatsu R13194 photomultiplier tube (PMT) detectors at the heart of each Tri-TIP instrument. First, dark current characteristics were determined for each detector at a wide range of operating temperatures using a vacuum thermal chamber. Second, the relative responsivity of each detector to visible and ultraviolet wavelengths above 200 nm was determined using a combination of an FEL lamp and deuterium lamp along with a series of bandpass interference filters. Finally, the responsivity of each detector at far ultraviolet (FUV) wavelengths was determined, specifically at 135.6 nm, the target wavelength for the Tri-TIP instrument. The FUV tests were carried out in the NRL vacuum UV calibration facility.

All three laboratory tests were conducted to determine several factors needed for the data analysis methodology. Several scale factors are required to subtract signals in each channel from one another. A chi-squared analysis was used to determine the best fit based upon the long wavelength test results. PMTs were paired based on the analysis and then assigned to a specific Tri-TIP unit depending upon the observing geometry. Sensitivity at FUV wavelengths was then used determine the placement of PMTs within each optical channel. Finally, each pair was grouped with a suitable third detector based on their dark noise characteristics and the selection results are summarized.

This page intentionally left blank.

DETECTOR SELECTION METHODOLOGY FOR THE TRIPLE-TINY IONOSPHERIC PHOTOMETER (TRI-TIP) INSTRUMENT

1. INTRODUCTION

The Triple Tiny Ionospheric Photometer (Tri-TIP) instrument has been developed by the Geospace Science and Technology Branch at the U.S. Naval Research Laboratory. Tri-TIP is the third generation of remote sensing instruments designed to detect far ultraviolet (FUV) emissions of atomic oxygen in the nighttime ionosphere. [1] Recent technological developments have reduced the size of Tri-TIP to a 1U CubeSat form factor (10 cm $\times$ 10 cm $\times$ 10 cm). [2] Four Tri-TIP instruments will be flown as part of the Coordinated Ionospheric Reconstruction CubeSat Experiment (CIRCE). [3] The primary objective of CIRCE is to characterize the two-dimensional distribution of electrons in the orbital plane of the spacecraft with an emphasis on studying the morphology of the Equatorial Ionization Anomaly (EIA). [4]

The Tri-TIP optics enable high sensitivity measurements of O I 135.6 nm, which are then used to derive profiles of electron density in the ionosphere. [5] The detectors used in the Tri-TIP instrument are Hamamatsu R13194 Photomultiplier Tubes (PMTs). [6] The R13194 PMT uses a Cesium Iodide (CsI) photocathode behind a magnesium fluoride (MgF_2) window to detect FUV radiation with a peak sensitivity at 130 nm and a cutoff near 200 nm. A set of three matched PMTs is used to effectively isolate signals in the nighttime ionosphere due to O I 135.6 nm. The aim of this work is to find the optimal combinations of PMTs to enable correcting the UV signal for both long wavelength contamination and background dark counts in orbit. Several correction coefficients are required to properly subtract the red and background signals from the UV signal. The present memorandum documents the test process used to match and select PMTs for the flight Tri-TIP units and to derive the PMT correction factors.

1.1 Tri-TIP Optical Design

The Tri-TIP optical design is illustrated in Fig. 1A, using a simple line diagram to highlight the essential components. Light enters the instrument through a set of two simple baffles to reduce unwanted scattered light. An off-axis parabola (OAP) mirror reflects and focuses the incoming signal through both a heated filter and beam splitter before converging on the detector surfaces. Tri-TIP relies on the heated filter and beam splitter in conjunction to isolate the atomic oxygen spectral emission line, O I 135.6 nm.

The heated strontium fluoride (SrF_2) filter, which has heritage from the first two TIP generations, suppresses light at wavelengths shorter than 135.6 nm. Strong absorption eliminates any transmission due to H I 121.6 nm. Heating the SrF_2 filter substrate to 100 C shifts its sharp spectral cutoff longward to also suppress unwanted O I 130.4 nm emissions by a factor of 50. [5] The beam splitter then divides the filtered signal between two experimentally matched PMTs. A reflective coating (Al-MgF_2) is applied to 50% of the first beam splitter surface in a polka dot pattern to evenly distribute incoming signals between one PMT channel that monitors the total signal and a second PMT channel that measures contaminating radiation at longer wavelengths, or “red leak” contamination. A third PMT used to monitor dark current in the instrument is not shown in the line diagram but is indicated in Fig. 1B along with the matched set.

Manuscript approved May 28, 2020.

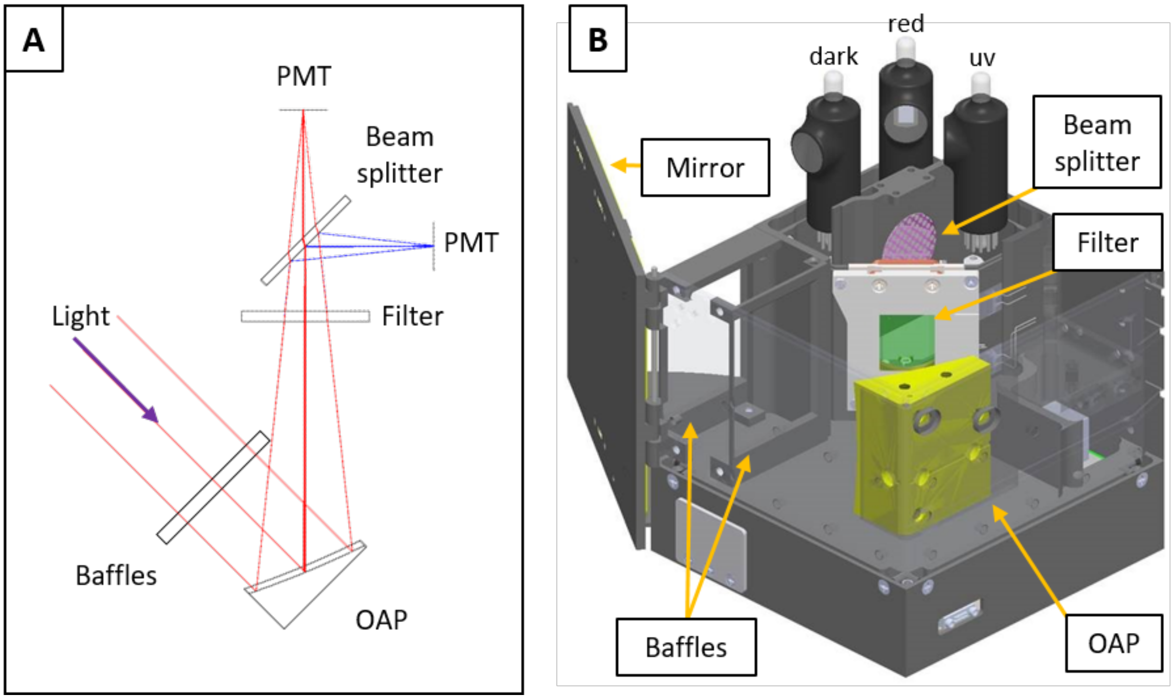

Fig. 1—Diagrams illustrate the primary instrument components that make up the primary Tri-TIP optics: (A) A line diagram illustrates the primary optical components. Light enters the system through two simple baffles, is focused by an off-axis parabolic mirror (OAP), passes through a heated filter, and is divided by a beam splitter prior to striking the PMT detector. (B) Partially exploded model further illustrates how the optical layout is packaged within a 1U CubeSat volume. An optional mirror used to select detector view angles is highlighted along with the individual PMT channels discussed in the text.

The sapphire beam splitter substrate transmits light at wavelengths longer than 142 nm to measure the "red leak." [5] Trace impurities in CsI photocathodes results in slight sensitivity to light at wavelengths above 200 nm in an otherwise nominally "solar blind" detector at visible wavelengths. The first generation of TIP sensors showed that moonlight reflected off clouds and city lights were visible in the data and required correction. [7] The red leak PMT measurement is subtracted from the UV PMT signal as part of the post-processing methodology to correct for this contamination. [8] In the special case where no long wavelength contamination is expected, for example when looking above the Earth's limb, the red leak correction is not necessary and both PMTs may be used to measure total UV signal by replacing the beam splitter sapphire substrate with MgF_2.

Table 1—Channel description for each PMT in the Tri-TIP instrument.

Channel	Description
1	dark
2	red
3	uv

1.2 Tri-TIP Data Analysis

The method used to isolate the target emission at O I 135.6 nm using three Tri-TIP channels was detailed in a prior memorandum and is reviewed briefly in this section. [8]. For consistency with the prior report, the

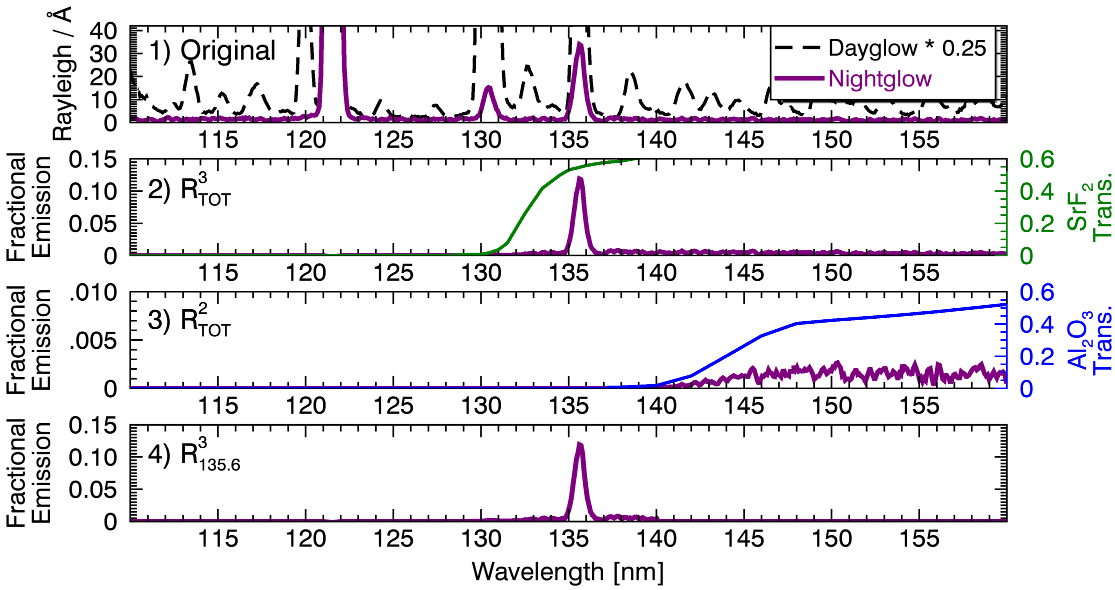

Fig. 2—The target passband of the Tri-TIP instrument is illustrated by showing examples of raw dayglow and nightglow spectra (Panel 1) acquired by the UVLIM instrument. [9] Panels 2 and 3 shows R^3_{TOT} and R^2_{TOT}, the nightglow spectral components measured by the uv and red channels, respectively. Panel 4 shows $R^3_{135.6}$, the desired result of filtering and post-processing.

three PMT channels are described as defined in Table 1, either numerically or in all lowercase letters (e.g. “uv”). Capitalized terms (e.g. “UV”) will be used when referring to corresponding signal inputs.

The event rate, R, in Channel 3 (Tri-TIP “uv” Channel) due to targeted UV emissions (counts s^{-1}) is represented by R^3_{UV}. The event rate is a function of $B_{UV}(\lambda)$, the surface brightness of UV emission line airglow in Rayleighs[1] and, $S_3(\lambda)$, the instrument sensitivity of Channel 3 (counts s^{-1} R^{-1}). The product $B_{UV}(\lambda)S_3(\lambda)$ is summed over all wavelengths in the instrument passband, assuming only discrete spectral emissions in this range.

$$R^3_{UV} = \sum_{\lambda} B_{UV}(\lambda)S_3(\lambda) \tag{1}$$

The Tri-TIP measurement goal is the event rate from the OI 135.6 nm doublet $(2p^{4\,3}P - 3s\ ^5S)$, or $R^3_{135.6} = B_{UV}(135.6)S_3(135.6)$. This measurement requires correcting for several potential unwanted signals. Panel 1 in Fig. 2 shows an example airglow spectrum in the FUV, including both a nightglow spectrum (solid purple) as the target for Tri-TIP and a dayglow spectrum (black dashed) for context. Panels 2 and 3 illustrate the spectral components measured by Channels 3 and 2, respectively, that represent the bulk of the expected total (R_{TOT}) signal in each channel. Panel 4 shows the effective bandpass of Tri-TIP used to determine $R^3_{135.6}$, which requires correcting for sources of noise and contamination.

[1]Rayleighs, R = 10^6 photons/s/cm^2/4π

$$R^3_{135.6} = R^3_{TOT} - R^3_{130.4} - R_{RED} - R_{DARK} \tag{2}$$

The full data reduction is abbreviated in Equation 2 to broadly summarize the information needed to determine $R^3_{135.6}$. [8] The raw total event rate measured in Channel 3 (R^3_{TOT}) is combined with data from the other two PMT channels to correct for unwanted contributions like red leak (R_{RED}) and dark noise in the system (R_{DARK}). First, assumptions are made about relative emission strength of unwanted spectral emissions (i.e. $R^3_{130.4}$). Pre-flight laboratory calibration provides confidence that the heated filter will eliminate any significant contribution due to OI 130.4 nm emissions. The term is retained as an acknowledgment to the potential contamination, though in flight it is typically assumed $R^3_{130.4} \approx 0$. Additional, out-of-band UV emissions are accounted for with the red leak correction term, R_{RED}.

$$R_{RED} = K_\eta \sigma R^2_{TOT} + \sum_{\lambda_j < 230} B_{NO}(\lambda_j)[S_3(\lambda_j) - K_\eta \sigma S_2(\lambda_j)] \tag{3}$$

The total event rate measured in the red channel, R^2_{TOT}, is scaled by two factors. The first, K_η, is a proportionality constant between detector efficiencies at wavelengths longer than 230 nm and is the most important consideration for matching PMTs within each Tri-TIP. The second constant, σ, combines several parameters outside the scope of this memo for the sake of brevity. The reflectivity/transmissivity ratio of the beam splitter (K_{bs}) and the instrument solid angles ($\Omega_{2,3}$) are condensed here as $\sigma = K_{bs}(\Omega_3/\Omega_2)$.

The red leak correction also explicitly includes terms for NO delta- and gamma-band nightglow emissions in the 190 nm $< \lambda <$ 230 nm wavelength band, represented by the sum over λ_j. The spectral response of the beam splitter transmittance and reflectance differ slightly at wavelengths shorter than 230 nm. [2] Determination of each channel sensitivity, $S_2(\lambda_j)$ and $S_3(\lambda_j)$, requires knowledge of the beam splitter spectral characteristics. The brightness of each emission band, $B_{NO}(\lambda_j)$, is scaled according to the relative difference between channel sensitivity to accurately remove red leak effects from the uv channel.

The third Tri-TIP channel is a fully enclosed PMT used to monitor sources of noise in the system, R_{DARK}, such as dark current. The signal measured in this channel, R^1_{TOT}, must scaled appropriately for use in the data reduction.

$$R_{DARK} = \{[d_3(T) - k_3] - K_\eta \sigma [d_2(T) - k_2]\} N^1_{PMT}(T) + [k_3 - K_\eta \sigma k_2] R^1_{TOT} \tag{4}$$

The temperature-dependent ratio, $d_i(T)$, relates the background noise rate between either the red ($i = 2$) or uv ($i = 3$) channel to the dark PMT channel, $N^1_{PMT}(T)$. Background noise rates were determined in thermal vacuum tests and ratios calculated for each set of PMTs after the selection of flight detectors. Noise generated by high energy charged particles is accounted for by the ratio of effective area for each detector, k_i. This factor is initially assumed to be a constant value, but will be validated during on-orbit testing.

To summarize, laboratory testing has been performed to determine the constants K_η and $d_{2,3}(T)$. These results were used as part of the selection criteria for detectors in the flight Tri-TIP instruments. Additional laboratory tests helped to identify detector sensitivity at the target UV wavelengths for Tri-TIP, another factor for consideration in flight component selection. The methodology and test results for determining the selection of flight PMTs are laid out in the following sections.

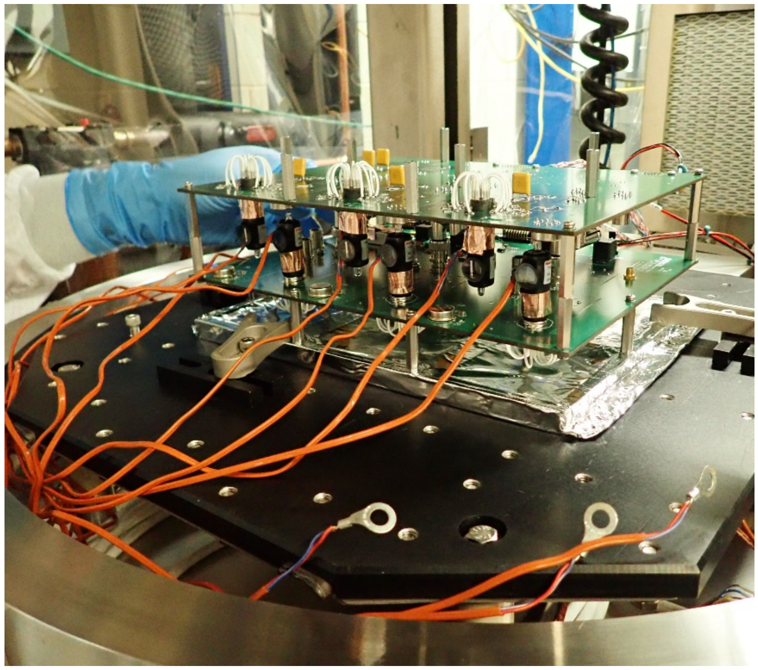

Fig. 3—Test setup for the dark count test inside the bell jar with thermistors (orange wires) attached to each PMT using copper tape for thermal conductivity

2. DARK COUNT TEMPERATURE PROFILE CHARACTERIZATION

Dark count rates, $N^i_{PMT}(T)$, were measured as a function of temperature for each Tri-TIP PMT. The count rates are used to determine the scale factor, $d_i(T)$, between the uv/red channels and the dark channel. This test is also important for identifying PMTs with aberrant behavior or with high rates of thermionic emission that would complicate data analysis. Characterization of dark count behavior early in the development process is important for identifying potentially noisy detectors.

2.1 Dark Count Test Approach

Tests were conducted inside a bell jar thermal vacuum system isolated from light contamination, including from internal sources (e.g. the ion gauge vacuum pressure sensor was turned off during testing). A set of test boards shown in Fig. 3 were used to power six detectors simultaneously with thermocouples affixed to each PMT to monitor the temperature. Dark counts were monitored at temperature set points between -20 C and +50 C, the Tri-TIP operating temperature range. Count rates were recorded for 10 minutes at each temperature once the system reached thermal equilibrium.

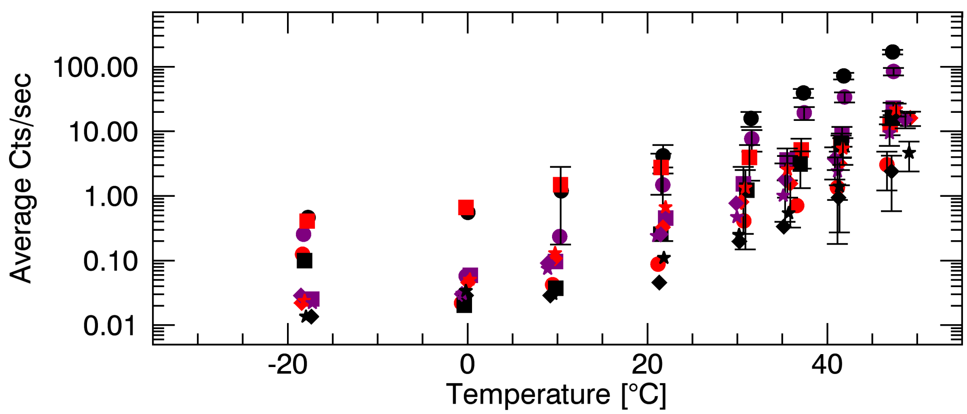

Fig. 4—Average dark count rate for the Hamamatsu R13194 PMTs used in the Tri-TIP flight units. Scatter points are color coded to represent the channel selected for each PMT (red, uv, dark). Different symbols (circle, square, diamond, and star) are used to represent separate Tri-TIP units. Error bars represent uncertainty due to counting statistics.

2.2 Dark Count Test Results

Figure 4 shows the dark current test results for twelve PMTs selected for Tri-TIP flight units out of the eighteen total PMTs that were tested. Ten of the eighteen PMTs tested showed minimal noise at room temperature and below (at or below 1 ct/sec). Two slightly noisier PMTs were also selected because their temperature profiles were well-behaved enough to use in data reduction. Three PMTs were ruled out entirely due to extreme noise levels or erratic behavior, and the remaining three PMTs are set aside as spare detectors.

The temperature dependence of the dark count rate within the CIRCE operating temperature range is roughly logarithmic. A few PMTs showed slightly higher counts at the lowest temperatures (-20 C), primarily due to noise generated by the solenoids engaging while cycling temperature controls. The noise source was identified shortly after the second round of three tests had begun. Active temperature controls were turned off for the remainder of the test and all subsequent low temperature tests, but the first batch of test results (six of eighteen PMTs) were contaminated by the external noise source at the lowest temperature.

3. ULTRAVIOLET RESPONSE CHARACTERIZATION

The relative sensitivities, $S_i(\lambda)$, of Tri-TIP PMTs were tested at wavelengths of primary interest for Tri-TIP (OI 130.4 nm and OI 135.6 nm). Hamamatsu test data sheets included with every PMT list several measurement data points (see Appendix A) but those do not include the Tri-TIP target wavelengths. The Hamamatsu test data sheet values for quantum efficiency (QE) are plotted as a box and whisker plot in Fig. 5 along with a typical QE spectral response curve derived from the Hamamatsu product sheet. [6] The box represents values between the bottom and top quartiles of QE, and a white line indicates the median.

3.1 UV Test Approach

Tests were conducted in the large vacuum UV calibration facility at the Naval Research Laboratory. [10] A hollow cathode gas discharge lamp was used with a He-H_2 gas mixture to generate an FUV continuum spectrum for PMT characterization across a range of wavelengths. The test board stack used in this test

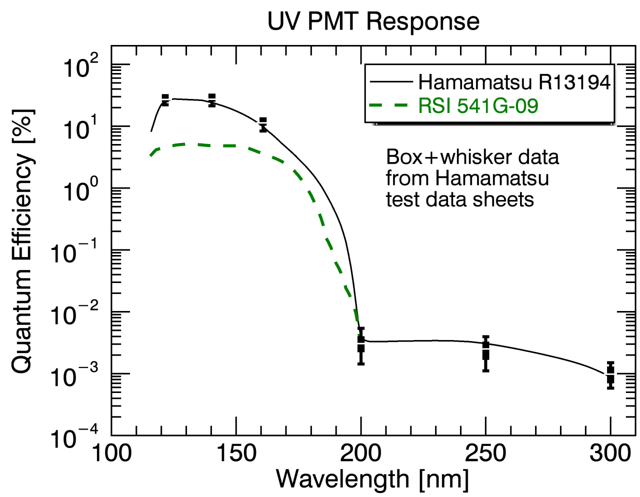

Fig. 5—Typical quantum efficiency (QE) curve for the Hamamatsu R13194 (black line) along with most recent calibrated curve for the RSI 541G-09 reference detector (green dash line). The QE for each PMT as listed in the Hamamatsu test data sheets are shown by the box and whisker plots.

was the same as the prior dark count tests (see Fig. 3). An RSI 541G-09 "G-tube" reference detector was used as a calibrated baseline to compare with the Hamamatsu detectors. A calibrated response curve for the G-tube is represented by the green dashed curve in Fig. 5 along with the Hamamatsu PMT information as a comparison. The G-tube measured the source illumination before and after each sequence of test data acquisition. Measurements were taken at multiple wavelengths, including 130.4 nm, 135.6 nm, and 140.0 nm for comparison with the Hamamatsu test data sheet value. Count rates, $C^{i}_{UV}(\lambda)$, were averaged over a 30 second exposure for each PMT for a given wavelength.

3.2 UV Test Results

The goal of the test was to verify the relative UV response, $R^{i}_{UV}(\lambda)$, as a function of wavelength, λ, and PMT (i). The G-tube measurements were used along with its QE response, QE_G, to determine an approximate QE of the Hamamatsu PMTs. First, the average count rate measured by the G-tube, $C_G(\lambda)$, was converted to an approximate incident signal, $S(\lambda)$.

$$S(\lambda) = \frac{C_G(\lambda)}{QE_G} \tag{5}$$

The incident signal, $S(\lambda)$, contains several assumptions but is used as an approximation of the true photon flux the G tube should detect. The true count rate may then be used to convert the count rates measured by the Tri-TIP PMTs, $C_{TIP}(\lambda)$, to a relative QE approximation, QE_{TIP}.

$$QE_{TIP} = \frac{C_{TIP}(\lambda)}{S(\lambda)} \tag{6}$$

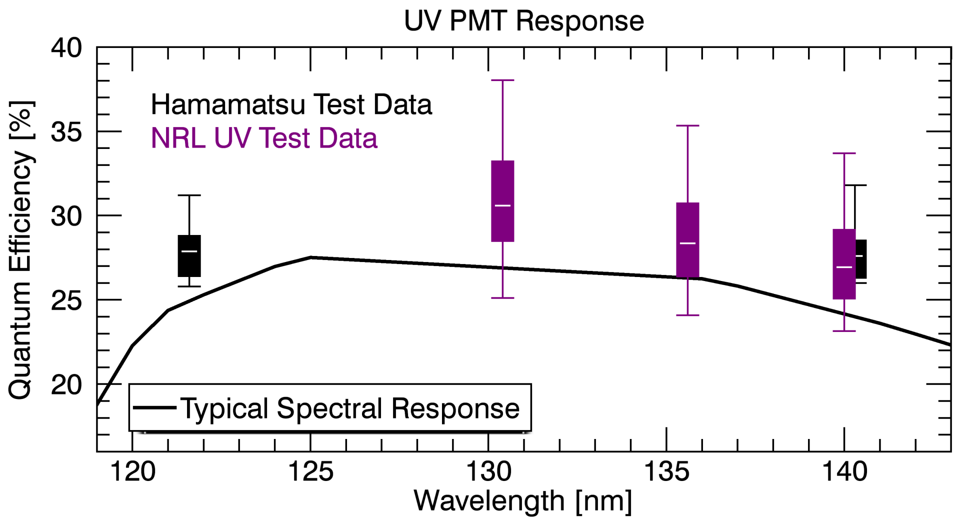

Fig. 6—Relative QE of the candidate flight PMTs for consideration in the CIRCE Tri-TIP units as tested for UV responsivity (purple), compared to the QE listed in the Hamamatsu test data sheets (black). The black curve is a baseline reference QE curve derived from the typical spectral response shown in the Hamamatsu product sheet.

One assumption made to determine $S(\lambda)$ is that the source illumination was uniform across the surface of the photocathodes, which are also assumed to have a uniform response. This assumption simplifies accounting for the relative sizes of the photocathode active area to a constant ratio between the QE values. The Hamamatsu R13194 photocathode has a 4 mm $\times$ 9.5 mm active area; the EMR G-tube has a circular 10 mm diameter active area (ratio = 2.07).

Relative QE values were then scaled based on a control PMT for consistency across tests to account for minor variability in experimental conditions (e.g. chamber pressures, source lamp stability). UV test results are summarized in Fig. 6 along with test data provided by Hamamatsu. Each box and whisker plot represents data for the 12 PMTs selected for CIRCE Tri-TIP flight units. Black box/whiskers represent the Hamamatsu QE test data at 121.6 nm and 140.6 nm. The purple box/whiskers at 130.4 nm, 135.6 nm, and 140.0 nm represent relative QE values calculated from the Tri-TIP PMT tests results.

The relative QE peaks at 130 nm as expected, though the spread in values is larger than the QE reported by Hamamatsu. Uncertainty in the QE calculation means that the data in Fig. 6 are best considered a relative comparison between detectors within each individual test. However, the relative response was deemed sufficient for purposes of PMT selection within the CIRCE Tri-TIP flight instruments.

4. RED LEAK RESPONSE CHARACTERIZATION

The most important factor in pairing PMTs for Tri-TIP is the relative sensitivity at longer wavelengths. Removing the red leak component, R_{RED}, from the uv channel signal, R^3_{TOT}, requires that the two CsI photocathodes respond similarly to long wavelength radiation. Experimental data showed the long wavelength spectral response of each PMT and allowed for determination of PMT pairs within each Tri-TIP to within the scaling factor, K_η.

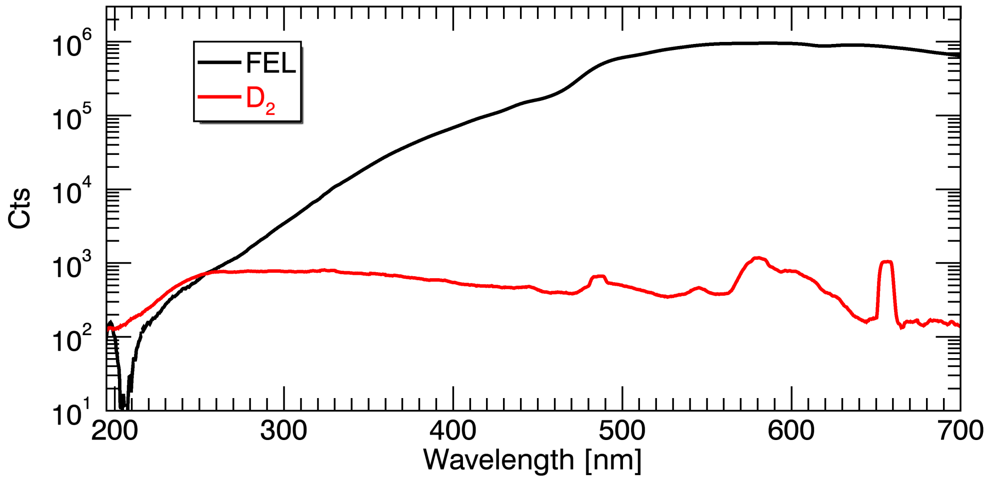

Fig. 7—Composite spectra represent the average output of each lamp used in the red leak test. Both spectra have been scaled to a 1 second integration time, background subtracted and smoothed over a 10 nm window using a boxcar smoothing routine. The FEL spectrum (black) is the average of 75 spectra taken over approximately 45 minutes of lamp operation; the D2 spectrum (red) the average of 50 spectra taken over approximately 30 minutes

4.1 Red Leak Test Approach

The goal of the red leak test was to determine the relative response, $R^i(\lambda)$, for each PMT (i) as a function of wavelength (λ). The red leak test was conducted at air on a laboratory optical table. PMTs were evaluated at wavelengths from 200-650 nm at 50 nm increments. Most of the tests were conducted with an FEL lamp, an ANSI standard 1000 Watt quartz halogen lamp (note: FEL is an ANSI designation, not an acronym). A deuterium (D_2) lamp was used to provide higher signal levels between 200-300 nm where the FEL lamp intensity drops off. Figure 7 shows spectra from both lamps averaged over multiple scans, background subtracted, and smoothed using a sliding, boxcar filter function over a 10 nm window.

Both lamps were directed to illuminate a $BaSO_4$ screen to fill common field of view for the detectors. The light was filtered using a set of bandpass interference filters from Edmund Optics. A commercial, off-the-shelf spectrometer (Ocean Optics USB2000) monitored the lamps for stability throughout the tests. Each PMT was exposed to the filtered lamp signal for each of the 10 test wavelengths, and count rates were averaged over 30 seconds.

4.2 Red Leak Test Results

The relative response of each PMT was calculated by dividing the average count rate recorded by each PMT, C^i_j, at a given wavelength ($j = 200, 250, \ldots, 650$ nm), by the expected spectral response, S_j.

$$R^i(\lambda) = \frac{C^i_j}{S_j} \tag{7}$$

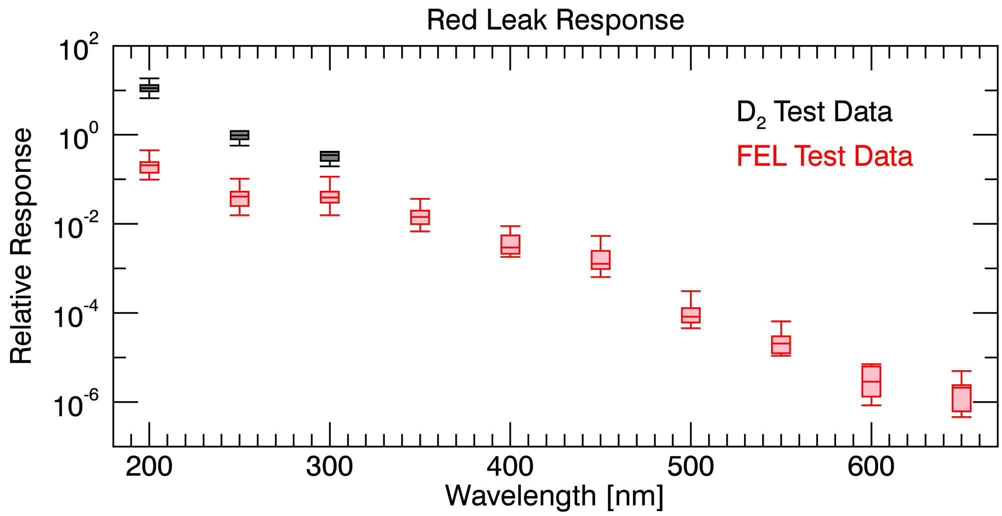

Fig. 8—Summary of test results showing the long wavelength sensitivity of the twelve Hamamatsu R13194 PMTs used in the CIRCE Tri-TIP flight units. Box and whisker plots show the relative response ($R^i(\lambda)$) as measured using both the deuterium (black) and the FEL lamp (red).

The spectral response at a given wavelength is determined by the brightness measured by the spectrometer, $B(\lambda)$ within the filter passband ($\pm\delta\lambda$) combined with the filter transmittance, $T(\lambda)$, and relative transmission of the spectrometer fiber optic, $F(\lambda)$.

$$S_j = \int_{\lambda_i-\delta\lambda}^{\lambda_i+\delta\lambda} T(\lambda)\frac{B(\lambda)}{F(\lambda)}d\lambda \tag{8}$$

Figure 8 summarizes the response of the PMTs chosen for the Tri-TIP flight units. All PMTs showed the same logarithmically decreasing response at wavelengths longer than 200 nm. The deuterium lamp provided higher count rates between 200-300 nm, and longward of 300 nm the FEL lamp signal is sufficient. The relative sensitivity varied by as many as eight orders of magnitude from 200-650 nm.

Standard deviation in the count rates is less than 10% everywhere and is less than 1% in the peak counting signal areas (350 nm–500 nm). Standard deviation in the lamp spectra used to determine the test sensitivity is also low, less than 1% at the peak and less than 20% at the extremes of the spectra. The most significant source of error in the results was due to a conservative uncertainty included in the filter response, a 20% error that accounts for the reported 2 nm reported tolerance in the FWHM specification.

5. PMT SELECTION

Selection of flight unit detectors for Tri-TIP started by matching the red leak responses of the detectors, the result of which is shown in Fig. 9. A weighted χ^2 analysis was used to determine the best fit between the relative responses of each PMT, scanning through scale factors, K_η. From the prior determined methodology [8], the scale factor relates the response of the uv channel ($\eta_{uv}(\lambda)$) and red channel ($\eta_{red}(\lambda)$).

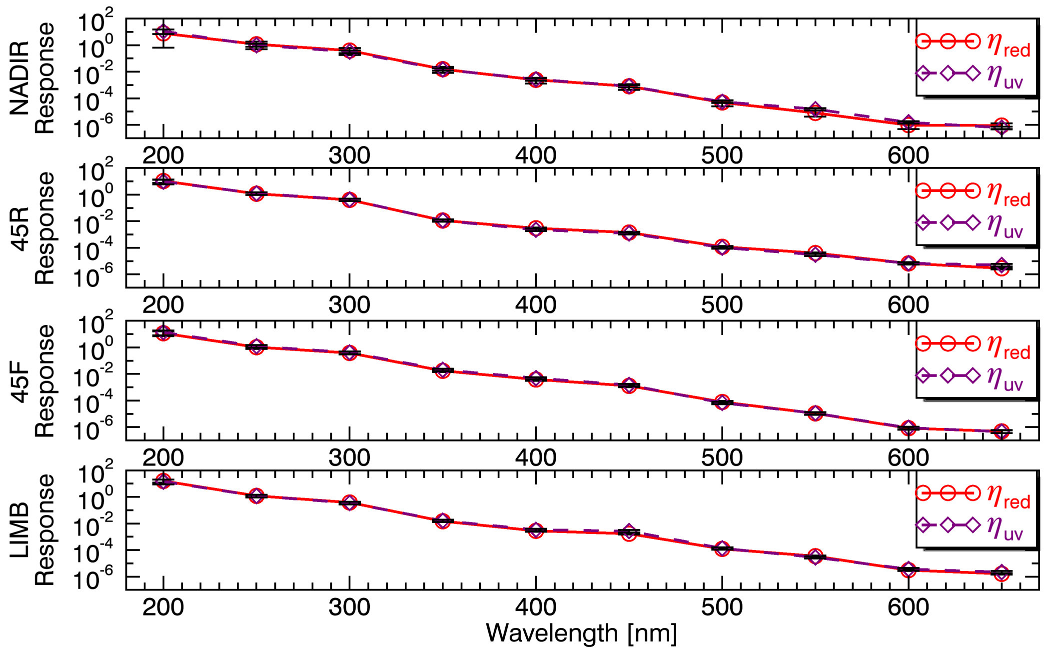

Fig. 9—Long wavelength response of the PMT pairs for each CIRCE Tri-TIP unit. The red channel response (η_{red}) has been scaled by the factor K_η to illustrate the match with the uv channel response (η_{uv}) in relative sensitivity across many orders of magnitude. Each red channel response is represented by red circles and each uv channel by purple diamonds.

$$K_\eta = \langle \frac{\eta_{uv}(\lambda)}{\eta_{red}(\lambda)} \rangle \tag{9}$$

Detector efficiencies, $\eta^i_{red}(\lambda)$ and $\eta^i_{uv}(\lambda)$, are represented by the relative response, $R^i(\lambda)$, determined in the red leak tests, where i represents the PMT. The factor, K_η, was varied and summed across all wavelengths, j, according to the following equation.

$$\chi^2_i = \sum_{j=200}^{650} W_j \frac{(R^{i'}_j - K_\eta R^i_j)^2}{K_\eta R^i_j} \tag{10}$$

The weight factor, W_j, approximates the mean lunar irradiance at full moon [11], which places a greater emphasis on matching the PMT response at wavelengths where moonlight reflected off cloud tops is the brightest. Reflected moonlight is expected to be the largest contributor to the red leak signal.

$$W_j = [0.5, 0.5, 0.75, 1.5, 3.0, 4.25, 4.25, 4.30, 4.35, 4.25]$$

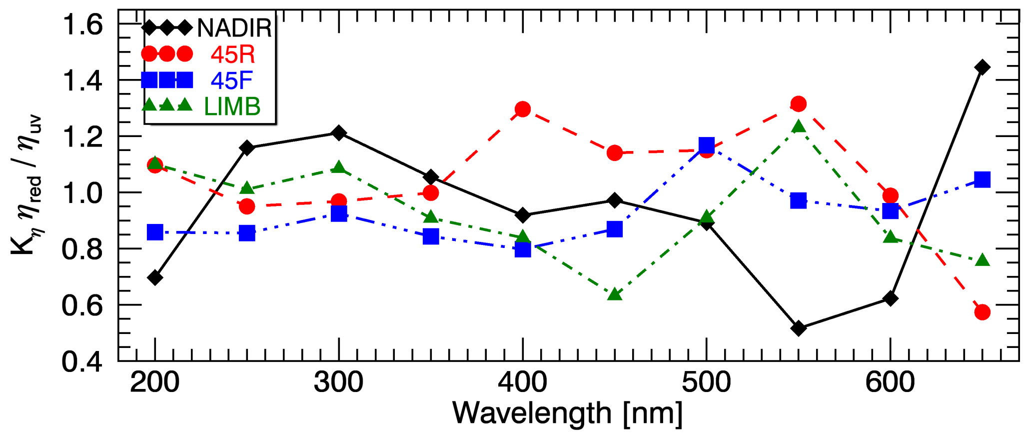

Fig. 10—A ratio representing the fit of each PMT pair, $K_\eta \eta_{red}(\lambda)/\eta_{uv}(\lambda)$, as a function of wavelength.

The factors, K_η, determined by the minimum of the weighted χ^2 analysis were applied to data acquired from both the FEL lamp and the D_2 lamp. Initial selection was made based on the best fit, or lowest χ^2 match between detectors. Table 2 lists the K_η values used to produce the optimized fit shown in Fig. 9. An ideal fit between detectors would produce a ratio value of $K_\eta = 1$ across all wavelengths, but the fit varies slightly as a function of wavelength. Figure 10 shows the ratio between detectors at each wavelength, $K_\eta \eta_{red}(\lambda)/\eta_{uv}(\lambda)$, based on the data illustrated in Fig. 9. A goodness of fit was then calculated based on the relative difference between each set of matched detectors.

$$\% = 100 \times \frac{K_\eta \eta_{red}(\lambda) - \eta_{uv}(\lambda)}{\eta_{uv}(\lambda)} \tag{11}$$

Table 2 lists the goodness of fit calculation results for the detectors selected for each flight Tri-TIP unit. Lower values represent a better fit between the two detectors at a particular wavelength. The D_2 measurements provide the data points from 200-300 nm where the signal levels are highest, and the FEL tests provide data from 350-650 nm. The goodness of fit results were used to select a detector pair for each Tri-TIP based on the particular viewing geometry.

Table 2—Goodness of fit (%) results for the Tri-TIP detectors

λ [nm]	200	250	300	350	400	450	500	550	600	650	K_η
NADIR	30.3	15.8	21.2	5.4	8.1	2.8	10.8	48.4	37.7	44.5	0.42
45R	9.6	5.0	3.2	0.2	29.6	14.0	15.0	31.5	1.2	42.6	1.38
45F	14.1	14.5	7.6	15.7	20.2	13.1	16.8	2.9	6.6	4.5	0.98
LIMB	10.0	1.1	8.5	9.1	16.1	36.7	9.0	23.0	16.3	24.6	1.53

The NADIR pair was selected because of the superior fit at 450 nm where the detector response is roughly two orders of magnitude higher than 550 nm (see Fig. 9). The NADIR unit will likely have the strongest red leak contamination concern due to its viewing geometry, so this was given priority. The 45R

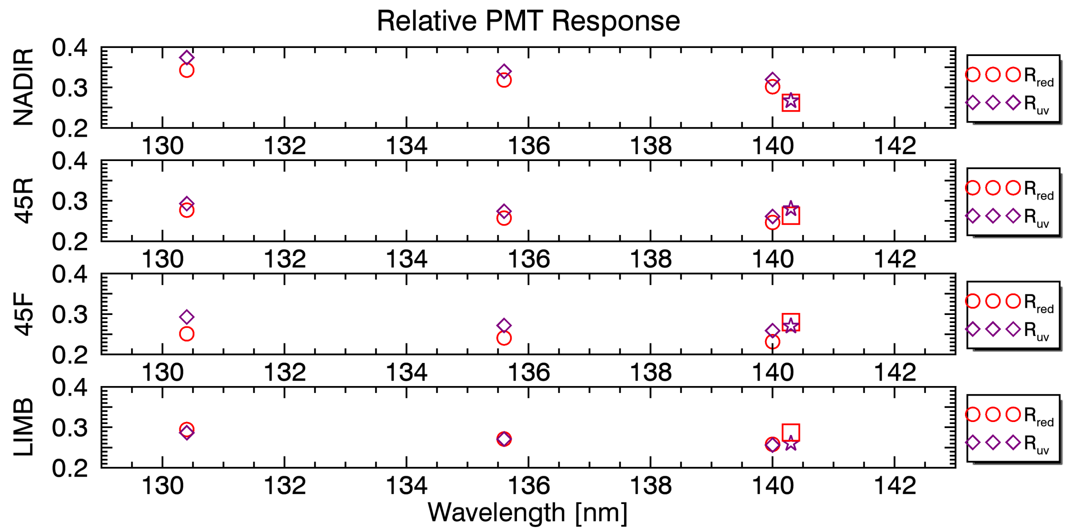

Fig. 11—Relative response for each pair of flight Tri-TIP PMTs are compared at multiple wavelengths. Test results from the NRL vacuum chamber are shown by the purple diamonds (uv channel) and red circles (red channel). QE values in this wavelength range, as specified in the test data sheets provided by Hamamatsu, are shown by the purple star (uv channel) and red box (red channel).

and 45F PMT pairs were chosen next for their overall goodness of fit based on the χ^2 statistics, with the LIMB PMT pair resulting from the remaining set. The LIMB Tri-TIP data will not require the red leak correction, but results are shown for completeness.

Once PMT pairs were assigned, UV sensitivity was used to selected which of the two PMTs was placed in each channel. Figure 11 compares the relative response at ultraviolet wavelengths for each flight pair of PMTs. Purple diamonds represent the lab test response of the PMT selected for the uv channel, and red circles represent the same for the red channel. For comparison, the one data point from the Hamamatsu test data sheets that falls in the wavelength region of primary interest is plotted as well. The manufacturer's quantum efficiency (QE) of the red channel PMT at 140.3 nm is represented by the red box, and the uv channel is represented by the purple star.

Agreement between laboratory testing and the Hamamatsu test data sheet values is good, but the lab test results were the primary deciding factor in the event of any minor discrepancies. For example, Tri-TIP units that require red leak subtraction (NADIR, 45R, 45F) fill the uv channel with the PMT most sensitive at 135.6 nm. This determination was made using the test data for all units in light of the slight discrepancy in the 45F unit at the nearest provided QE value at 140.3 nm. The LIMB Tri-TIP simply placed the more UV sensitive PMT in the red channel position to help offset transmission losses through the beam splitter substrate.

The final PMT selection in the Tri-TIP flight units was for the dark channel, which was determined by matching the remaining available PMT behavior with the pairs already chosen for channels 2 and 3. Dark count rates from Fig. 4 were used to match each PMT pair with a suitable third detector. The dark count test results were then used to determine the scaling factors, $d_2(T)$ and $d_3(T)$, as a function of temperature.

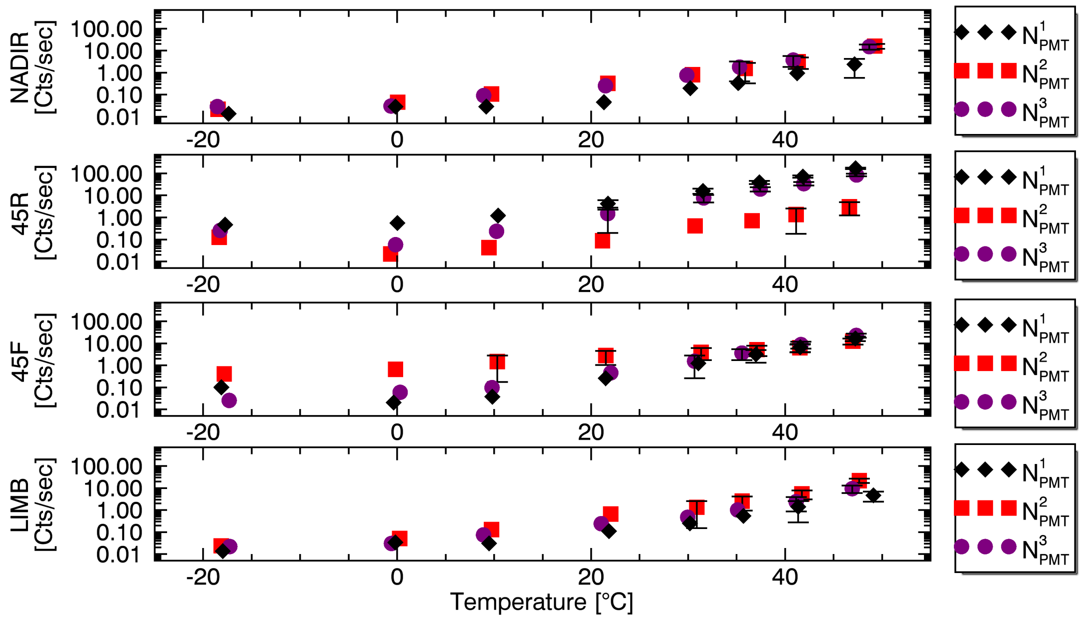

Fig. 12—Temperature dependence of dark count rates is shown for each PMT within the four flight Tri-TIP units. Dark channel (black diamonds), red channel (red boxes), and uv channel (purple circles) dark count rates are shown for their respective units.

$$d_{2,3}(T) = \frac{N^{2,3}_{PMT}(T)}{N^1_{PMT}(T)} \tag{12}$$

Noise measured on the dark channel, $N^1_{PMT}(T)$, will be used to subtract any noise from both the red channel, $N^2_{PMT}(T)$, and the uv channel, $N^3_{PMT}(T)$. When possible, the uv channel was given priority in terms of fit. Limited stock of flight quality detectors required matching each dark channel PMT as best as possible with the available inventory. Table 3 lists the ratios calculated for each combination of PMT selection for Tri-TIP.

Table 3—Dark count ratios as a function of temperature for each PMT set in the flight Tri-TIP units

	Temp.	-20 C	0 C	10 C	22 C	30 C	36 C	42 C	50 C
NADIR	d_2	1.63	1.59	3.76	7.19	4.08	4.64	3.35	6.71
	d_3	2.13	1.06	3.18	5.56	3.88	5.36	3.97	6.31
45R	d_2	0.27	0.04	0.04	0.02	0.03	0.02	0.02	0.02
	d_3	0.55	0.10	0.20	0.35	0.48	0.49	0.47	0.50
45F	d_2	4.08	32.75	40.18	10.77	3.21	1.66	0.95	0.77
	d_3	0.25	2.92	2.59	1.76	1.26	1.15	1.32	1.38
LIMB	d_2	1.75	1.50	4.28	6.06	5.38	4.71	3.87	4.69
	d_3	1.63	0.90	2.44	2.18	1.89	1.87	1.71	2.01

Figure 12 illustrates the dark noise behavior for each PMT used to compute the values in Table 3. Dark counts for each red channel are represented by red squares, the uv channel by purple circles, and the dark channel by the black diamonds. Data points near -20 C in each of the 45 units show the anomalously high noise levels due to the test setup (see Section 2.2). The 45F and 45R units also illustrate our preference for matching the dark channel most closely with the uv channel when given the opportunity.

6. SUMMARY

Guidelines for selecting flight detectors for the CIRCE Tri-TIP instruments were derived from the data analysis methodology laid out in a prior memorandum [8]. The relevant driving principles are summarized throughout this memo and were used to shape the tests described herein. Red leak matching was prioritized, followed by relative sensitivity in the ultraviolet, and finally dark count characteristics. Final PMT selections are listed in Table 4.

The CIRCE mission will use four Tri-TIP instruments, spread across two 6U CubeSats, to provide four separate viewing angles on the ionosphere. Understanding the behavior of each PMT within an individual Tri-TIP instrument is critical for effective data reduction. This memorandum detailed the process of determining two important parameters for the data reduction process via laboratory testing and how those parameters were used to determine the final flight configuration.

Table 4—Final PMT selection for each CIRCE Tri-TIP Channel (uv, red, dark)

CIRCE	Tri-TIP	Ch. #	Name	PMT S/N
Trail	NADIR	1	dark	DAZ 0628
		2	red	DAZ 0652
		3	uv	DAZ 0653
Trail	45R	1	dark	DAZ 0608
		2	red	DAZ 0547
		3	uv	DAZ 0597
Lead	45F	1	dark	DAZ 0594
		2	red	DAZ 0613
		3	uv	DAZ 0619
Lead	LIMB	1	dark	DAZ 0661
		2	red	DAZ 0630
		3	uv	DAZ 0627

ACKNOWLEDGMENTS

B. A. Fritz is an NRC Postdoctoral Research Associate resident at the U.S. Naval Research Laboratory.

REFERENCES

1. S. Budzien, B. Fritz, A. Stephan, P. Marquis, S. Powell, B. O'Hanlon, A. Nicholas, K. Dymond, and C. Brown, "Comparison of second and third generation 135.6 nm ionospheric photometers using on-orbit and laboratory results," in T. S. Pagano, C. D. Norton, and S. R. Babu, eds., *CubeSats and SmallSats for Remote Sensing III*, volume 11131, 2019 (International Society for Optics and Photonics, SPIE), 2019, pp. 1 – 13. doi:10.1117/12.2528791. URL `https://doi.org/10.1117/12.2528791`.
2. B. A. Fritz, A. W. Stephan, P. W. Walker, C. M. Brown, A. C. Nicholas, K. F. Dymond, S. A. Budzien, P. J. Marquis, T. T. Finne, and K. D. Wolfram, "Ultraviolet beam splitter characterization for use in a CubeSat optical system," *Journal of Applied Remote Sensing* **13**(3), 1 – 11 (2019), doi:10.1117/1.JRS.13.032503. URL `https://doi.org/10.1117/1.JRS.13.032503`.
3. A. C. Nicholas, G. D. R. Attrill, K. F. Dymond, S. A. Budzien, A. W. Stephan, B. A. Fritz, G. J. Routledge, J. A. Miah, C. M. Brown, P. J. Marquis, T. T. Finne, C. N. Mitchell, R. J. Watson, D. O. Kataria, and J. Williams, "Coordinated Ionospheric Reconstruction CubeSat Experiment (CIRCE) mission overview," in T. S. Pagano, C. D. Norton, and S. R. Babu, eds., *CubeSats and SmallSats for Remote Sensing III*, volume 11131 (International Society for Optics and Photonics, SPIE), 2019, pp. 105 – 117. doi:10.1117/12.2528767. URL `https://doi.org/10.1117/12.2528767`.
4. K.F. Dymond, A.C. Nicholas, S.A. Budzien, A.W. Stephan, P. Marquis, C.M. Brown, T. Finne, and K.D. Wolfram, "Low-latitude ionospheric research using the CIRCE Mission: instrumentation overview," *Proc. SPIE, UV, X-Ray, and Gamma-Ray Space Instrumentation for Astronomy XX* **10397** (2017), doi:10.1117/12.2275336. URL `https://doi.org/10.1117/12.2275336`.
5. A. W. Stephan, P. J. Marquis, S. A. Budzien, K. F. Dymond, C. M. Brown, K. D. Wolfram, and A. C. Nicholas, "Evaluation of UV optics for triple tiny ionospheric photometers on CubeSat missions," *Proc. SPIE, CubeSats and NanoSats for Remote Sensing II* **10769** (2018), doi:10.1117/12.2321042. URL `https://doi.org/10.1117/12.2321042`.
6. *R13194 Photomultiplier Tube* (Hamamatsu, 12 2015). TPMS1088E01.
7. S.A. Budzien, K.F. Dymond, C. Coker, and D.H. Chua, "Tiny Ionospheric Photometers on FORMOSAT-3/COSMIC: on-orbit performance," *Proc. SPIE, Solar Physics and Space Weather Instrumentation III* **7438** (2009), doi:10.1117/12.826532. URL `https://doi.org/10.1117/12.826532`.
8. S. A. Budzien, A. W. Stephan, K. F. Dymond, C. M. Brown, P. J. Marquis, and A. C. Nicholas, "Three-Channel Airglow Photometer Data Analysis Methodology," U.S. Naval Research Lab, Washington, D.C., U.S., 2018.
9. S. A. Budzien, P. D. Feldman, and R. R. Conway, "Observations of the far ultraviolet airglow by the Ultraviolet Limb Imaging Experiment on STS-39," *Journal of Geophysical Research: Space Physics* **99**(A12), 23275–23287 (12 1994), ISSN 0148-0227, doi:10.1029/94JA01543. URL `https://doi.org/10.1029/94JA01543`.

10. P. C. Kalmanson, C. Sarner, and S. E. Thonnard, "Facilities for the calibration, construction, and environmental testing of instruments and detectors in the EUV and FUV," in A. M. Larar and M. G. Mlynczak, eds., *Optical Spectroscopic Techniques, Remote Sensing, and Instrumentation for Atmospheric and Space Research IV*, volume 4485 (International Society for Optics and Photonics, SPIE), 2002, pp. 303 – 315. doi:10.1117/12.454265. URL `https://doi.org/10.1117/12.454265`.

11. S. D. Miller and R. E. Turner, "A Dynamic Lunar Spectral Irradiance Data Set for NPOESS/VIIRS Day/Night Band Nighttime Environmental Applications," *IEEE Transactions on Geoscience and Remote Sensing* **47**(7), 2316–2329 (July 2009), doi:10.1109/TGRS.2009.2012696.

This page
intentionally
left blank

Appendix A

MANUFACTURER TEST DATA SHEET INFORMATION

Manufacturer provided information from Hamamatsu

Table A1—Quantum Efficiency (%) of Hamamatsu R13194 detectors considered for Tri-TIP (Supply Voltage = 1000 V)

λ [nm]	121.6	140.3	160.8	200	250	300	GAIN ($\times 10^6$)
DAZ 0547	27.5	26.3	10.7	2.49E-03	2.69E-03	1.18E-03	1.24
DAZ 0588	28.0	27.1	10.8	2.65E-03	1.68E-03	7.30E-04	1.63
DAZ 0594	29.8	28.9	11.9	5.41E-03	3.94E-03	1.25E-03	2.56
DAZ 0597	28.8	28.0	11.4	2.85E-03	3.14E-03	1.25E-03	1.80
DAZ 0608	28.8	26.3	10.5	1.43E-03	1.11E-03	5.80E-04	3.29
DAZ 0613	28.0	28.0	11.1	3.92E-03	3.25E-03	1.13E-03	1.84
DAZ 0617	30.7	30.1	12.1	2.88E-03	2.77E-03	1.14E-03	3.16
DAZ 0619	26.7	27.0	11.4	2.99E-03	1.93E-03	8.60E-04	2.37
DAZ 0622	29.2	28.6	11.8	2.80E-03	3.50E-03	1.30E-03	3.21
DAZ 0627	26.0	26.0	10.3	2.98E-03	1.67E-03	6.80E-04	3.16
DAZ 0628	31.2	31.8	12.9	4.29E-03	2.77E-03	1.44E-03	2.50
DAZ 0630	28.7	28.7	11.4	1.59E-03	1.31E-03	5.80E-04	2.01
DAZ 0652	26.9	26.2	10.5	3.08E-03	2.35E-03	1.04E-03	1.40
DAZ 0653	26.3	26.7	11.2	2.60E-03	2.10E-03	8.00E-04	2.58
DAZ 0658	27.2	26.6	10.9	2.90E-03	1.70E-03	8.00E-04	2.52
DAZ 0661	25.8	27.3	11.4	2.00E-03	1.50E-03	6.00E-04	2.28

Table A2—Radiant Sensitivity (A/W $\times 10^3$) of Hamamatsu R13194 detectors considered for Tri-TIP (Supply Voltage = 1000 V)

λ [nm]	121.6	140.3	160.8	200	250	300
DAZ 0547	33.4	36.9	17.2	4.98E-03	6.73E-03	3.54E-03
DAZ 0588	44.6	49.8	22.8	6.95E-03	5.52E-03	2.88E-03
DAZ 0594	75.0	83.9	39.4	2.24E-02	2.03E-02	7.73E-03
DAZ 0597	50.6	56.8	26.6	8.27E-03	1.14E-02	5.43E-03
DAZ 0608	92.8	98.2	44.7	7.61E-03	7.34E-03	4.60E-03
DAZ 0613	50.5	58.4	26.4	1.16E-02	1.21E-02	5.00E-03
DAZ 0617	94.9	107.4	49.3	1.47E-02	1.76E-02	8.70E-03
DAZ 0619	62.1	72.5	35.0	1.15E-02	9.20E-03	4.90E-03
DAZ 0622	92.0	104.0	49.0	1.47E-02	2.25E-02	1.04E-02
DAZ 0627	80.5	93.1	42.1	1.52E-02	1.06E-02	5.20E-03
DAZ 0628	76.4	89.8	41.6	1.73E-02	1.40E-02	8.70E-03
DAZ 0630	56.5	65.2	29.6	5.20E-03	5.30E-03	2.80E-03
DAZ 0652	36.9	41.5	19.1	7.00E-03	6.60E-03	3.50E-03
DAZ 0653	66.5	77.9	37.5	1.09E-02	1.11E-02	5.20E-03
DAZ 0658	67.2	75.6	35.5	1.17E-02	8.80E-03	5.10E-03
DAZ 0661	57.6	70.5	33.7	7.50E-03	6.90E-03	3.40E-03